International Journal of Electrical and Computer Engineering (IJECE)
Vol. 9, No. 2, April 2019, pp. 771~782
ISSN: 2088-8708, DOI: 10.11591/ijece.v9i2.pp771-782

Operational performance of a PV generator feeding DC shunt and induction motors with MPPT

Mohammed I. Abuashour[1], Tha'er O. Sweidan[2], Mohammad S. Widyan[3], Mohammed M. Hattab[4], Mohammed A. Ma'itah[5]
[1,3,4.5]Department of Electrical Engineering, Faculty of Engineering, the Hashemite University, 13115, Zarqa, Jordan
[2]Electrical Engineering Department, Higher Colleges of Technology, Sharjah Women's College 7947 Sharjah, United Arab Emirates

Article Info

Article history:

Received Apr 1, 2018
Revised Nov 4, 2018
Accepted Nov 30, 2018

Keywords:

Induction motor
DC shunt motor
MPPT
PV generator
Transient analysis
Steady state analysis.

ABSTRACT

This paper presented the transient and operational behavior of a parallel Combination of DC Shunt Motor and IM fed by a photovoltaic generator at different solar irradiance levels. The maximum power point of current/voltage (I/V) characteristic of the PV generator was achieved for different solar intensities, by utilizing an open circuit voltage method. The nonlinear operational behavior of (I/V) characteristics of the PV generator at various solar intensities and the magnetization curve of the ferromagnetic material of the DC shunt motor were both modeled by high order polynomial mathematical expressions. The study investigated the response of the system at different solar irradiance levels and changing the torque loads for both motors and then following step change in solar intensity levels with fixed loading torques for both motors. All numerical simulations were executed using MATLAB software.

Corresponding Author:

Mohammed I. Abuashour,
Department of Electrical Engineering,
The Hashemite University,
13115, Zarqa, Jordan.
Email: Mohammedi@hu.edu.jo

1. INTRODUCTION

The dramatic increase in the world's population elevates the demand for electricity to comply with their numerous different applications. So many researchers have focused recently on this lively concern. Additionally, the environmental considerations and many other related issues have boosted the attention and the awareness for the use of renewable energy resources for example wind, solar, fuel cells, water power and many others as measures for this anticipated critical crisis and deficiency in many countries [1]. Furthermore, the overall objective of renewable energy systems is to obtain electricity that is cost competitive and even advantageous with respect to other energy sources [2].

So the necessity for studying the renewable energy resources like the photovoltaic system operational characteristics under various loads (DC and AC) in transient and steady state conditions has become crucial in assisting the design and the correct implementation of such systems.

The simulated stability investigations for standalone photovoltaic energy systems are presented [3]-[7]. The simulations are taken for different types of DC motors. Controllers of different types are utilized to guarantee the system stability under different loadings and irradiance levels, also and Analysis on the Impact of Renewable Energy to Power System Fault Level is presented [8].

In this paper, the proposed system is an autonomous PV generator for feeding simultaneously DC load (DC shunt motor) and AC load (three phase IM) and the stability analysis in the transient and steady states are conducted. In this work an open circuit voltage technique is used to track the maximum power

point of the PV generator through changing the duty cycle of the DC-DC buck-boost power converter to keep the output voltage of DC-DC buck boost converter equal to the value of voltage at maximum power point of the I/V characteristic of PV generator at all solar irradiance levels. This paper is organized in the following ways: Section 2 presents the configuration and description of the system under study. The numerical simulations and discussions are addressed in Section 3 and finally conclusions are presented in Section 4

2. SYSTEM CONFIGURATION AND DESCRIPTION

Figure 1 shows the schematic diagram for the stand-alone PV solar energy system. It is a PV panels feeding a parallel combination of loads the DC shunt motor and IM. The PV generator is designed by connecting many modules in series and parallel so as to attain the rated values for DC shunt motor and IM. DC-DC buck-boost power converter is used as a common stage between PV generating unit and both DC shunt motor and IM to force the voltage to the corresponding value related to the MPP at all solar irradiance levels by adjusting the duty cycle D.

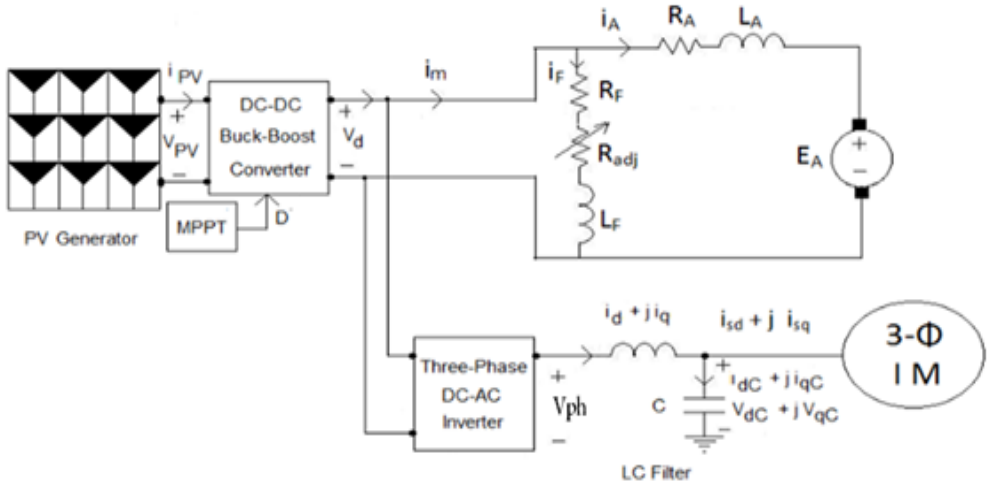

Figure 1. Schematic diagram for the system under study

2.1. PV generator design and system dynamical model

This section presents some design characteristics of the PV generator along with its output characteristics which are the terminal voltage of the PV generator as function of the output current and the corresponding output power at various solar irradiance levels. The mathematical equations representing the dynamics of the DC shunt motor, LC filter, Voltage controller and IM are also summarized.

2.1.1. Photovoltaic design and output characteristics

The mathematical model of PV array is given by following Equation [9], [10].

$$I_L = N_p I_{Ph} - N_p I_o \left[\exp\left(\frac{q}{HKT} * \frac{V_O}{N_s}\right) - 1\right] \quad (1)$$

Where I_L is PV array output load current (A), V_O is PV array output voltage (V), N_s is Number of series PV cell and N_p
Is the Number of parallel PV cells. The PV array output power is given by,

$$P = V_O * I_L = V_O * \left(N_p I_{Ph} - N_p I_O \left[\exp\left(\frac{q}{HTA} * \frac{V_O}{N_s}\right) - 1\right]\right) \quad (2)$$

The PV solar power plant is designed so that its maximum power ratings at full solar intensity comply with the operational ratings of both motors using PV modules made by AVANCIS Company. It consists of modules connected in parallel and in series combinations to achieve the desired values for current, voltage and power. Here the PV generator has a power of 14.2 kW, an open-circuit voltage of about

585.6 V and a short-circuit current of about 36.9A. The voltage and current at MPP are 448.2 V and 31.68 A, respectively. It consists of 18 parallel branches and each branch has 9 modules connected in series. The voltage and power versus current of the designed PV generator at different solar irradiance levels are shown in Figure 2.

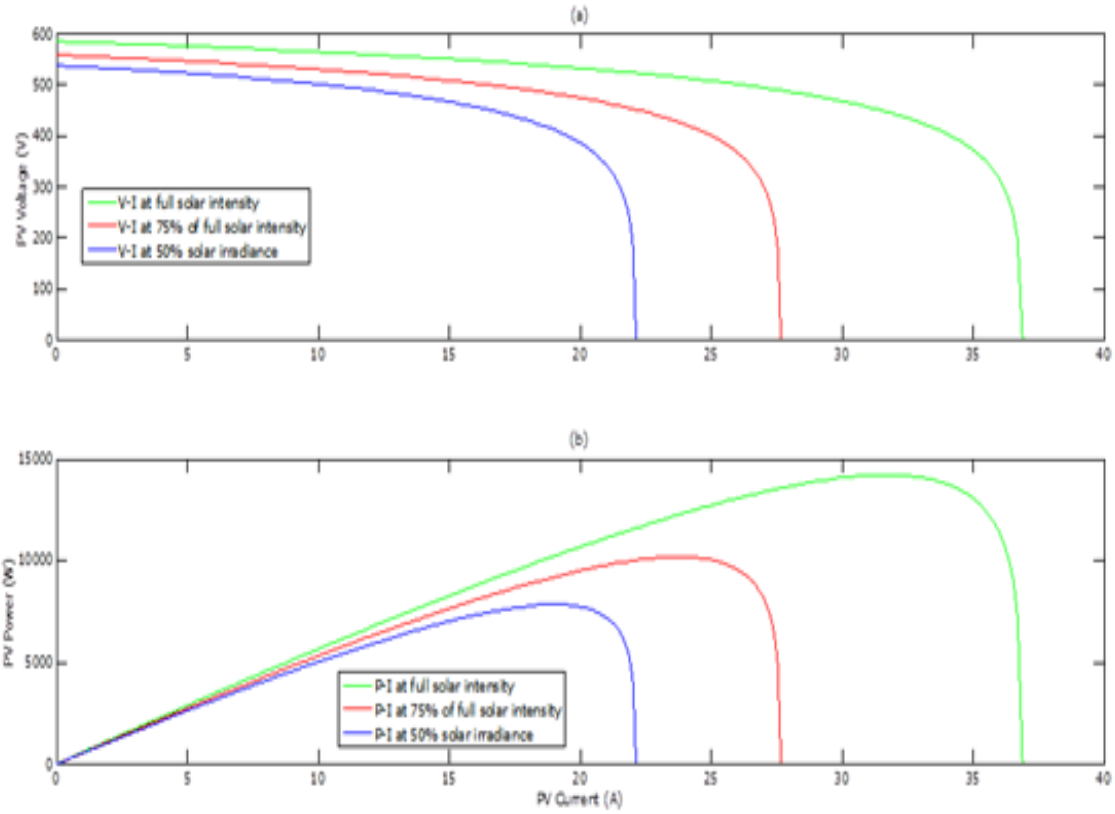

Figure 2. (a) PV voltage as function of the output PV current of the designed PV generator at various solar irradiance levels and (b) The corresponding output power

It can be clearly noted from Figure 2(a), the output PV voltage as function of the current of the PV generator is highly nonlinear. It has been approximated using a 10th order polynomial function using MATLAB as [11]:

$$V_{PV} = \sum_{n=1}^{11} \alpha_n I_{PV}^{11-n} = \alpha_1 {I_{PV}}^{10} + \alpha_2 {I_{PV}}^{9} + \alpha_{11} \quad (3)$$

$$I_{PV} = I_A + I_F + \sqrt{(i_d)2 + (i_q)2} \quad (4)$$

2.1.2. Dynamical Mathematical Model for DC Shunt Motor

In DC shunt motor, the field and the armature circuits are connected in parallel. The nonlinear dynamical mathematical model of DC shunt motor is [12]:

$$K\phi = \sum_{n=1}^{8} \alpha_n {I_F}^{8-n} = \alpha_1 {I_F}^{8} + \alpha_2 {I_F}^{7} + \alpha_8 \quad (5)$$

$$L_F \frac{di_F}{dt} = V_d - i_F(R_F + R_{adj}) \quad (6)$$

$$L_A \frac{di_A}{dt} = V_d - i_A R_A - K\phi W \quad (7)$$

$$J\frac{d_\omega}{dt} = K\phi i_A - T_L \quad (8)$$

In Equations (7) & (8) $K\phi$ is not a state variable and it varies nonlinearly with the field current of the DC shunt motor. It has been approximated using 7th order polynomial as it has been already given in Equation (5). The results of the polynomial curve fitting are shown in Figure 3.

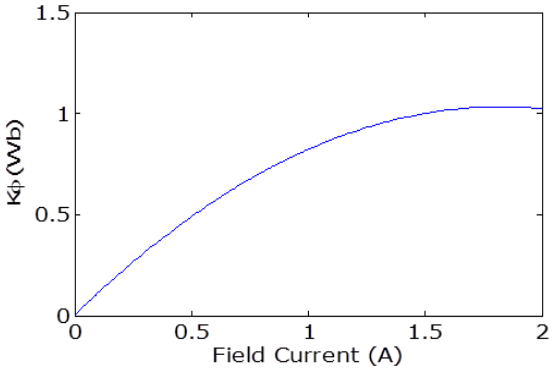

Figure 3. The nonlinear polynomial curve fitting of 7th order degree for ferromagnetic material

2.1.3. Dynamical mathematical model for three-phase induction motor

The nonlinear dynamical mathematical model of squirrel cage three-phase induction motor in synchronously rotating d-q reference frame can be summarized as [13]:

$$L_{ssm}\frac{di_{sdm}}{dt} + L_{mm}\frac{di_{rdm}}{dt} = V_{dsm} + \omega_s L_{ssm} i_{sqm} + \omega_s L_{mm} i_{rqm} - R_{sm} i_{sdm} \quad (9)$$

$$L_{ssm}\frac{di_{sqm}}{dt} + L_{mm}\frac{di_{rqm}}{dt} = V_{qsm} - \omega_s L_{ssm} i_{sdm} - \omega_s L_{mm} i_{rdm} - R_{sm} i_{sqm} \quad (10)$$

$$L_{mm}\frac{di_{sdm}}{dt} + L_{rrm}\frac{di_{rdm}}{dt} = V_{dr} + (\omega_s - \omega_{rm}) L_{rrm} i_{rqm} + (\omega_s - \omega_{rm}) L_{mm} i_{sqm} - R_{rm} i_{rdm} \quad (11)$$

$$L_{mm}\frac{di_{sqm}}{dt} + L_{rrm}\frac{di_{rqm}}{dt} = V_{qr} - (\omega_s - \omega_{rm}) L_{rrm} i_{rdm} - (\omega_s - \omega_{rm}) L_{mm} i_{sdm} - R_{rm} i_{rqm} \quad (12)$$

$$J_m\frac{d\omega_{rm}}{dt} = \frac{3P_m}{4}\left(L_{mm} i_{rdm} i_{sqm} - L_{mm} i_{rqm} i_{sdm}\right) - T_{Lm} \quad (13)$$

$$\frac{d\delta_r}{dt} = \frac{(\omega_s - \omega_{rm})}{\omega_s} \quad (14)$$

2.1.4. Dynamical Mathematical Model for the LC Filter

Applying KVL& KCL around the loop of the inductance and the capacitance of the filter in the system in d-q reference frame yields [13]:

$$C\frac{dV_{Cd}}{dt} = I_{din} - i_{sdm} + \omega_s C V_{Cq} \quad (15)$$

$$C\frac{dV_{Cq}}{dt} = I_{qin} - i_{sqm} - \omega_s C V_{Cd} \quad (16)$$

$$L\frac{dI_{din}}{dt} = \frac{D}{1-D} V_{PV} \sin(\delta_{PV}) + \omega_s L I_{qin} - V_{Cd} \quad (17)$$

$$L\frac{dI_{qin}}{dt} = \frac{D}{1-D} V_{PV} \cos(\delta_{PV}) - \omega_s L I_{din} - V_{Cq} \quad (18)$$

$$\tan(\delta_{PV}) = \frac{-\omega_s L I_{q_{in}} + V_{Cd}}{\omega_s L I_{d_{in}} + V_{Cq}} \quad (19)$$

2.1.5. Voltage controller

As shown in Figure 1, the process of controlling the voltage of the PV generator and thus controlling the voltage of the common coupling point is represented by Equation (20) [12]:

$$T_D \frac{dD}{dt} = \frac{V_{set}}{V_{PV}+V_{set}} - D \quad (20)$$

The DC-DC buck boost converter is a power electronic device used to change the average value of the input voltage into higher, equal or lower value. They are used extensively in regulated power supplies, electrical motor drive systems and renewable energy resources as an intermediate stage for controlling purposes. The output voltage of buck boost converter is controlled by changing the duty cycle D of its switch [14]. Duty ratio D is defined as the ratio between the ON mode duration of the switch t_{on} and the total switching duration T_s. It runs in the boost mode when D is greater than 0.5 where the average value of the output voltage becomes greater than the input voltage. The buck mode takes place if D becomes less than 0.5. Mathematically, the output voltage V_O as function of the input voltage V_{PV} is given by:

$$V_d = \frac{D}{1-D} V_{PV} \quad (21)$$

The open circuit voltage of the PV generating unit is being measured while the switch of DC-DC power converter is in open state. The MPP is sought in the range of 0.73 to 0.8 of its open circuit voltage [15].For this paper it has been used as 0.78, the measurement process of the open circuit voltage is [11]:

$$T_m \frac{dV_{set}}{dt} = 0.78V_{PV-OC} - V_{set} \quad (22)$$

The inverter is fundamentally a power electronic device that changes DC to AC. The inverter power is provided by a DC input source. Inverters find applications in uninterruptible power supply (UPS) systems, motor drives and renewable energy systems. Inverters typically use pulse width modulation (PWM) method which is a highly developed technique where the width of the gate pulses is controlled by various mechanisms to achieve certain purposes [14]. Harmonics in the output voltage of the sinusoidal PWM inverters are always there and therefore filters are normally connected across the output terminals of inverters to filter those unwanted harmonics. The line to line voltage can be expressed as:

$$V_{LL} = \frac{\sqrt{3}}{2\sqrt{2}} m_a V_d \quad (23)$$

Equations (6–18), (20) and (22) represent the complete nonlinear dynamical mathematical model of the proposed system. The nomenclature and the numerical parameters, ratings and specifications are given in Appendix A. The constants of the polynomial curves of Equation (3) and (5) are given in Appendix B.

3. NUMERICAL SIMULATIONS AND RESULTS

This section presents the numerical simulations and the results of the system into two different cases firstly with full solar intensity, and 50 % of full solar intensity and different loading conditions for both motors. Secondly with a fixed load while the solar intensity levels are being step changed.

3.1. System response at full solar irradiance level and different loading conditions

Figure 4 shows the system response at full solar intensity as the load torque of the DC shunt motor has been step changed from 12 Nm to 10N.m. The resulting field current is 2.046A; the armature current has changed as follows 9.834A at load of 12 N.m while at 10N.m is 8.274 A, The DC Shunt motor rotational speeds are at 12 N.m is 3563rpm, and 3581 rpm at 10N.m. The DC Shunt motor voltage is 448.5V. Like wise the IM load torque has been step changed from 25Nm to 20 Nm. The phase voltage during this step change is kept at 138.9V. The stator current is 16.8A at 25 N.m while at 20 Nm is 15.07 A. Meanwhile its rotational speed is 1782 rpm at 25N.m, and 1789 rpm at 20Nm.

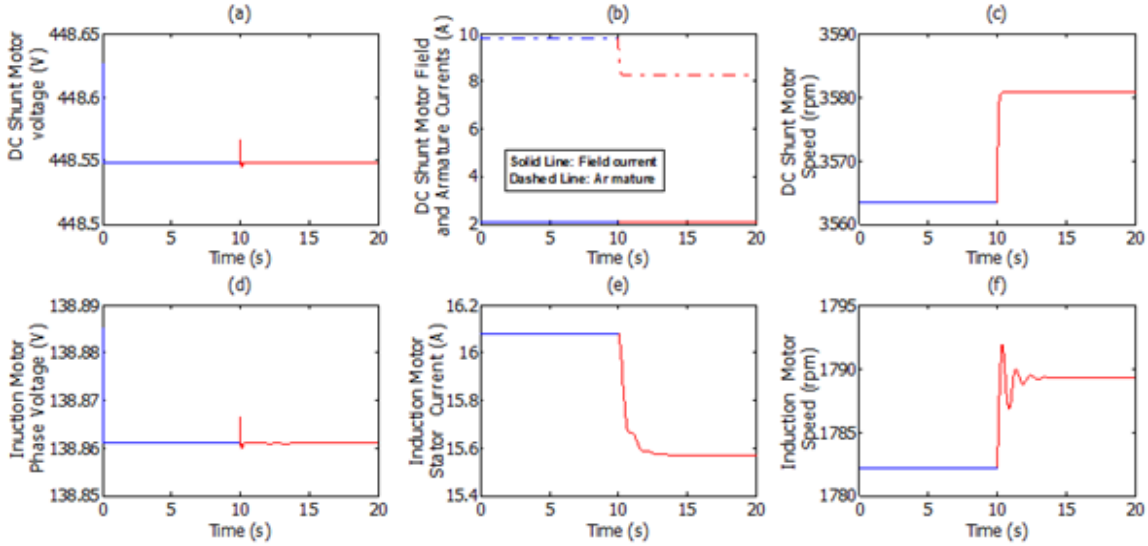

Figure 4. DC Shunt motor voltage, its field current, its armature current and its rotational speed. IM phase voltage, IM stator current and IM rotational speed variations after step change in load torque from (12-10) N.m for DC Shunt motor and from (25-20) N.m for IM at full irradiance level (a) DC Shunt motor voltage (b) DC Shunt motor field current and armature current (c) DC Shunt motor rotational speed (d) IM phase voltage (e) IM stator current (f) IM rotational speed

Figure 5 illustrates the PV system various quantities during the step change in the load torques at full solar intensity. The PV current has changed from 27.06A to 24.99 A, the duty cycle has changed from 0.49555 to 0.491, and PV terminal voltage has changed from 500V to 509V. The system complex power has changed from 13.53 KVA to 12.72 KVA, the IM active power is 5.143 kW at 25 N.m and 5.327 kW at 20 N.m. Correspondingly the active power of DC Shunt motor is 4.563 kW at 12N.m and 4.629 at 10N.m. The system total reactive power has changed from 8.611 to 8.397 (KVAr).

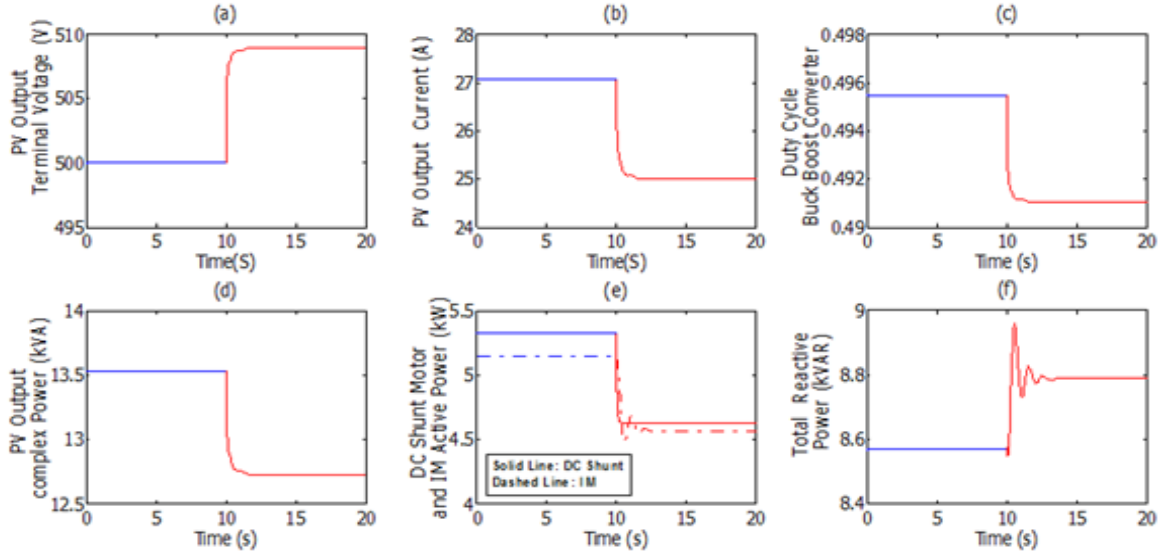

Figure 5. System various values variations after step change for IM load torque from (25-20) N.m and from (12-10) for DC Shunt motor at full solar irradiance level (a) PV terminal voltage (b) PV output current (c) System duty cycle (d) PV output complex power (e) DC Shunt motor and IM active power (f) System total reactive power

3.2. System response at 50% of full solar irradiance level and different loading conditions

Figure 6 shows the system response at 50% of full irradiance level as the load torque has been step changed for the DC shunt motor from 6N.m to 4N.m. The resulting field current is 1.71A. The armature current variations are as follows at 6 N.m is 5.266A while at 4N.m is 3.659 A. Meanwhile DC shunt motor rotational speed at 6 N.m is 3420 rpm, and 3445 rpm at 4N.m. Correspondingly the DC Shunt motor voltage is 412.5V. The IM the load torque has been step changed from 10N.m to 6 N.m. The resulting phase voltage is 127.7V, the stator current is as follows at 10 N.m is 14.03A while at 6N.m is 13.96 A. Meanwhile IM and rotational speeds are at 10N.m is 1795rpm, and 1797 rpm at 6N.m.

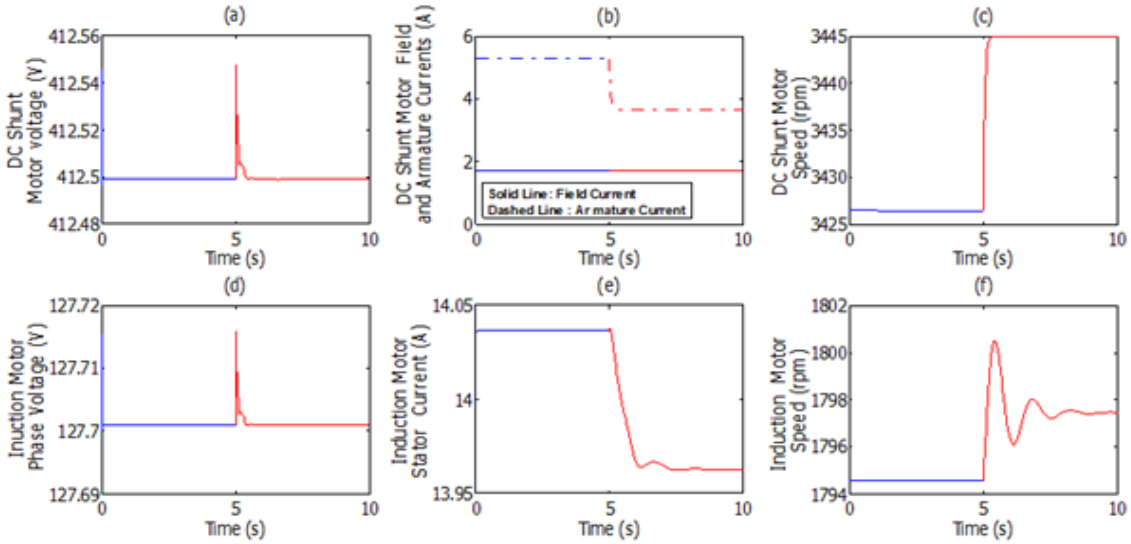

Figure 6. DC Shunt motor voltage, its field current, its armature current and its rotational speed. IM phase voltage, IM stator current and IM rotational speed variations after step change in load torque from (6-4) N.m for DC Shunt motor and (10-6) N.m for IM at 50% of full irradiance level (a) DC Shunt motor voltage (b) DC Shunt motor field current and armature current (c) DC Shunt motor rotational speed (d) IM phase voltage (e) IM stator current (f) IM rotational speed

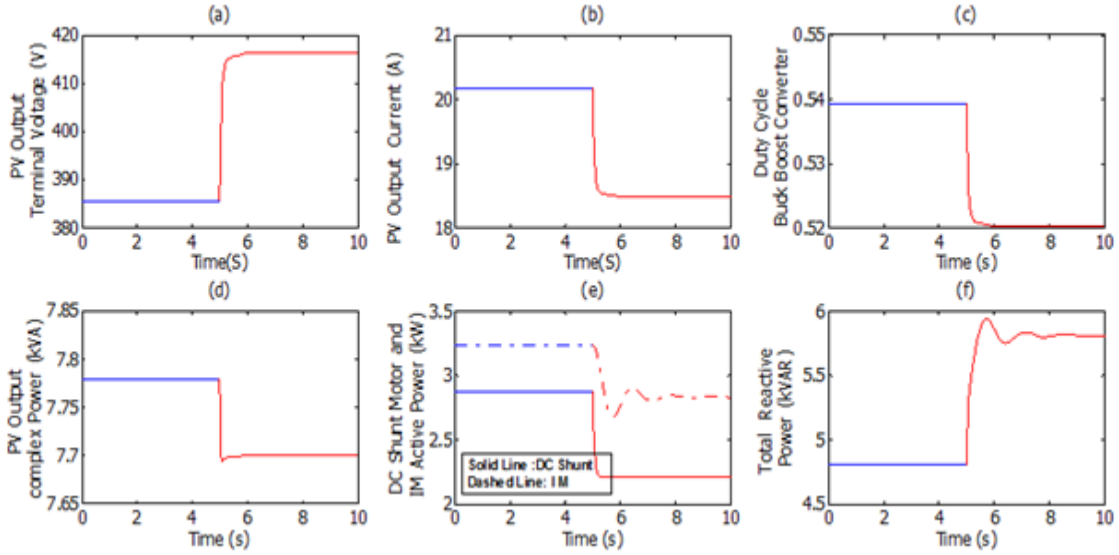

Figure 7. System various values variations after step change for IM load torque from (10-6) N.m and from (6-4) for Dc Shunt motor at 50% of full irradiance level (a) PV terminal voltage (b) PV output current (c) System duty cycle (d) PV output complex power (e) DC Shunt motor and IM active power(f) System total reactive power

Figure 7 illustrates the PV system various electrical quantities variations at 50% of full irradiance level. The PV current has changed from 20.17 to 18.49A, the duty cycle has also changed from 0.534 to 0.5202 and its terminal voltage has changed from 385.6V to 416.4V. The system complex power has changed from 7.78 KVA to 7.7 KVA. At 10 N.m the IM motor active power is 3.327kW and at 6N.m is 2.833kW. Correspondingly the active power of DC Shunt motor 2.877kW at 6 N.m and 2.215 kW at 4N.m load torque. The system total reactive power ranges from 4.811 to 5.812 (KVAr).

3.3. The Response of the system after a successive step changes in solar irradiance levels and a fixed load torque of 10N.m for IM and 6 N.m for DC shunt motor

Figure 8 reveals the response of the system as it has been subjected to a successive step changes in solar irradiance levels from the Full irradiance intensity passing into 75% of full irradiance intensity and then finally passing through 50% of full irradiance intensity. The DC Shunt Motor voltages during this step change are as follows 448.5, 428.2 and 412.5V, respectively. The resulting field currents during this step change are 2.046, 1.86 and 1.71A respectively, the resulting armature currents during this step change are 5.160, 5.212 and 5.266A respectively and meanwhile DC Shunt motor rotational speeds are 3615, 3507 and 3426 rpm respectively. While the load torque for IM is fixed to 10N.m and 6 N.m for DC Shunt motor. The phase voltage for IM is 138.9, 132.6 and 127.7V, respectively, its rotational speed is 1796, 1795 and 1795rpm, respectively and its stator current is 15.23, 14.56 and 14.04A respectively.

Figure 9 represents the PV system various values variations as it is subjected to a successive step changes in solar irradiance levels. The PV generating unit output terminal voltages are 522.9, 472.8 and 385.6V, respectively and its output currents are 21.52, 20.76 and 20.18A, respectively. While the duty cycle of buck boost converter is step changed in the following fashion 0.4843, 0.4979 and 0.5349, respectively. The system complex powers are 11.25, 9.815 and 7.78KVA, respectively and the DC Shunt motor active powers are 3.3.32, 3.029 and 2.877 kW, respectively. Correspondingly IM active powers are 3.676, 3.423 and 3.236 kW, respectively. The system total reactive powers are 8.884, 7.396 and 4.812 (KVAr), respectively.

Figure 10 represents the torque-speed characteristics for the induction motor and the DC shunt motor at full irradiance level and a load torque of 25N.m for IM and 12N.m for the DC shunt motor which complies strongly as it is compared with the well-known characteristics of the electrical machines operation in general (The higher the load torque the lower the speed).

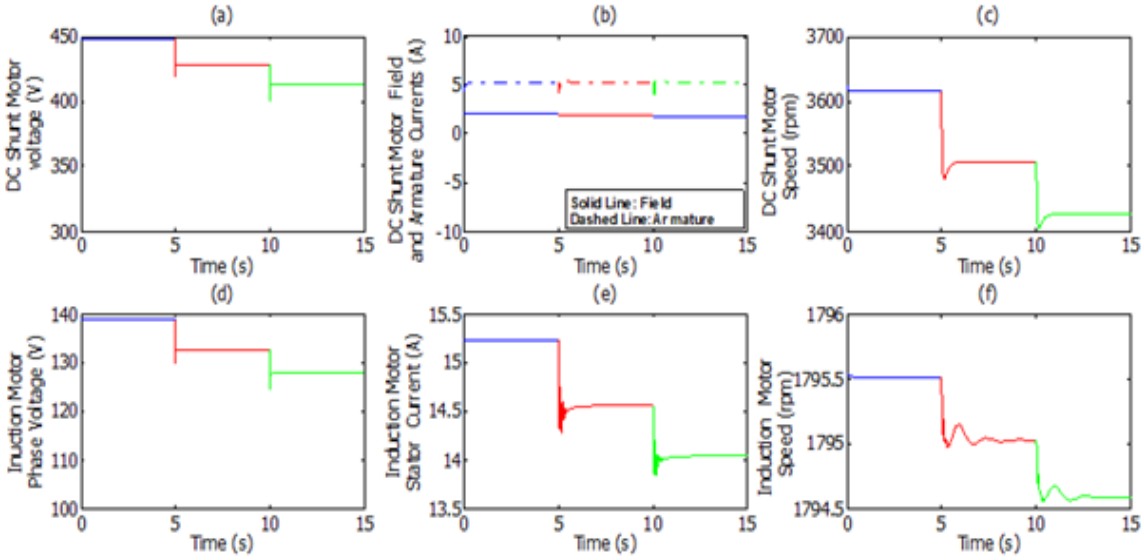

Figure 8. DC Shunt motor voltage, its field current, its armature current and its rotational speed. IM phase voltage, IM stator current and IM rotational speed variations after successive step changes of the solar irradiance levels from full intensity to 75% to 50% of full intensity and the load torque for IM is fixed to 10N.m and 6N.m for DC Shunt motor (a) DC Shunt motor voltage (b) DC Shunt motor field current and armature current (c) DC Shunt motor rotational speed (d) IM phase voltage (e) IM stator current (f) IM rotational speed

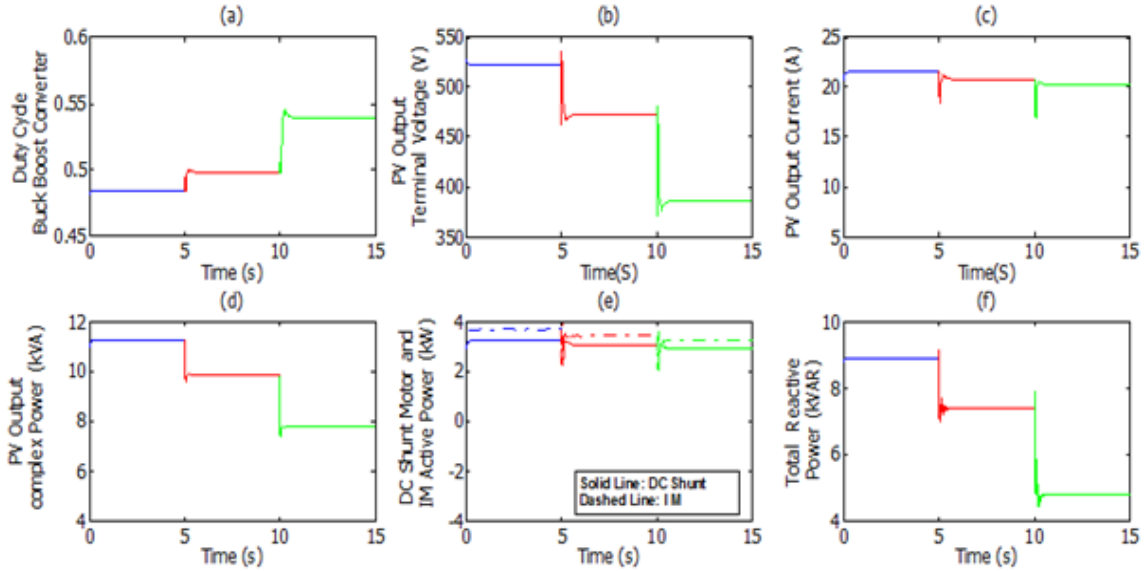

Figure 9. System various values variations after successive step changes of the solar irradiance levels from full intensity to 75% to 50% of full intensity and the load torque for IM is fixed to 10N.m and 6N.m for DC Shunt motor (a) System duty cycle (b) PV terminal voltage (c) PV output current (d) PV output complex power (e) DC Shunt motor and IM active power (f) System total reactive power

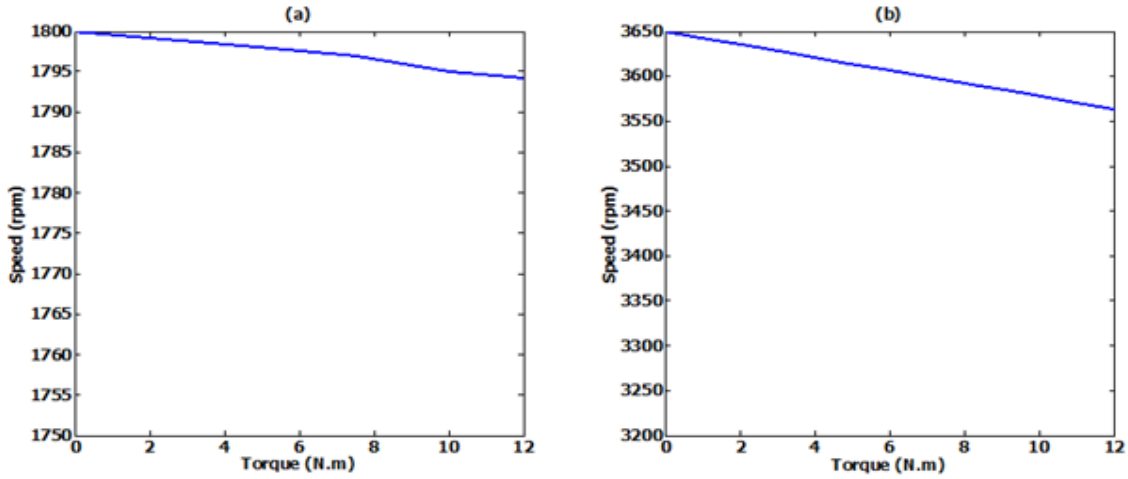

Figure 10. (a) The torque speed characteristics of Induction motor (b) The torque speed characteristics of DC shunt motor

4. CONCLUSION

The transient and the operational behavior of a parallel Combination of DC Shunt Motor and IM fed by a photovoltaic generator at different solar irradiance levels are presented. The PV generator feeds a parallel combination load of DC shunt and IM. The PV generator is designed and connected at a common coupling point which in turn feeds the two motors. The integration of the PV generator to the IM is accomplished via DC-DC buck-boost switch mode power converter; three-phase inverter and LC filter to suppress the inherent harmonics available in the output voltage of the inverter. In addition, the integration of the PV generator to the DC Shunt Motor is accomplished through the same DC-DC buck-boost. The DC-DC converter is used to maintain constant voltage corresponding for the MPP of PV generator at the common coupling point via adjusting its duty cycle. The study comprises the response of the power system after step changes in the load coupled to both motors at two solar irradiance levels and after successive step changes in the solar intensity with constant motor loading conditions. It is concluded that the DC-DC converter runs all the time in buck-boost (step-down and step up) modes and the proposed power system can run steadily at

wide range of solar intensity levels and motors loading conditions with common coupling point voltage very close to the nominal maximum power point. Moreover, the output power from the PV generator has widely changed in accordance to the level of solar intensity. In all cases, it is found that the power consumed by both motors is equal to the total power generated by the PV generator. Basically, as the mechanical load coupled to both motors increases, the rotational speed of the motor decreases and the stator and the armature currents rise. As a general conclusion, the proposed standalone power system can withstand step changes in the load coupled to the motors and step changes in the solar irradiance levels which indicates the robustness and proves the reliability of the integration between the different system components.

Appendix A

Table A1. Nomenclature

Variable	Explanation	Variable	Explanation
D	Duty cycle of buck boost converter		
C	Capacitance of the LC filter	R_{sm}	Induction motor stator resistance
V_{Cd}&V_{Cq}	D&Q axis components of the voltage across the capacitors, respectively	L_{ssm}	Induction motor stator inductance
I_d & I_q	D&Q axis components of inverter output current, respectively	L_{mm}	Induction motor mutual inductance between its stator and rotor windings
L	Inductance of the LC filter	R_{rm}	Induction motor rotor resistance
δ_{PV}	Delta angle of the voltage injected by the PV generator	L_{rm}	Induction motor rotor inductance
I_{cd}&I_{cq}	D&Q axis components of the capacitors current, respectively	i_{sdm}	D-axis component of induction motor stator current
ω_s	Synchronous radian frequency	i_{sqm}	Q-axis component of induction motor stator current
L_F	DC Shunt motor Field inductance	i_{rdm}	D-axis component of induction motor rotor current
ω	DC Shunt motor rotor speed	i_{rqm}	Q-axis component of induction motor rotor current
ω_{rm}	Induction motor rotor speed	P_m	Number of poles for induction motor
R_A	DC Shunt motor armature resistance	B	Rotor mechanical friction for induction motor
$R_A + R_{adj}$	DC Shunt motor Field plus the adjusted resistance	J_m	Moment of inertia of induction motor rotor and the load
L_A	DC Shunt motor armature inductance	V_{set}	The set voltage
i_F	DC Shunt motor Field current	T_M	Controller time constants
i_A	DC Shunt motor Armature current	PV	Photovoltaic
$K\phi$	DC Shunt motor flux	MPP	Maximum Power Point for photovoltaic array
T_L	DC Shunt motor Load torque	V_{OC}	Open circuit Voltage for photovoltaic array
J	Moment of inertia of DC Shunt motor rotor and the load	I_{SC}	Short circuit current for photovoltaic array
T_{Lm}	Induction motor Load torque	V_{MPP}	Voltage at MPP for photovoltaic array
V_{dsm}	D-axis component of induction motor stator voltage	I_{MPP}	Current at MPP for photovoltaic array
V_{qsm}	Q-axis component of induction motor stator voltage	I_{PV}	Photovoltaic array output current
V_{drm}	D-axis component of induction motor rotor voltage	IM	Induction motor
V_{qrm}	Q-axis component of induction motor rotor voltage	m_a	Inverter modulation index
i_{sqm}	Q-axis component of induction motor stator current	I_o	Reverse saturation current of the diode
i_{rdm}	D-axis component of induction motor rotor current	q	Electron charge = 1.6 * 10-19 Coulombs
i_{rqm}	Q-axis component of induction motor rotor current	H	Ideality factor
P_m	Number of poles for induction motor	K	Boltzmann constant = 1.38 * 10–23 Joule/°K
B	Rotor mechanical friction for induction motor	T	Temperature on absolute scale °K
J_m	Moment of inertia of induction motor rotor and the load	δ_r	Rotor angle of the Induction motor
i_{sqm}	Q-axis component of induction motor stator current	V_d	Inverter and DC shunt motor input voltage
i_{rdm}	D-axis component of induction motor rotor current	V_O	PV array output voltage
i_{rqm}	Q-axis component of induction motor rotor current	A	PV cell exposed area
P_m	Number of poles for induction motor	I_{Ph}	Light generated current
B	Rotor mechanical friction for induction motor	V_{PV-OC}	The open circuit voltage of PV generator
J_m	Moment of inertia of induction motor rotor and the load	V_{PV}	PV system terminal voltage
i_{sqm}	Q-axis component of induction motor stator current	V_{Ph}	Inverter phase voltage
i_{rdm}	D-axis component of induction motor rotor current	R_{sm}	Induction motor stator resistance
i_{rqm}	Q-axis component of induction motor rotor current	L_{ssm}	Induction motor stator inductance
P_m	Number of poles for induction motor	L_{mm}	Induction motor mutual inductance between its stator and rotor windings
B	Rotor mechanical friction for induction motor	R_{rm}	Induction motor rotor resistance
J_m	Moment of inertia of induction motor rotor and the load	L_{rm}	Induction motor rotor inductance
i_{sqm}	Q-axis component of induction motor stator current	i_{sdm}	D-axis component of induction motor stator current

Numerical System Parameters, ratings and specifications for the system:
Parameters of the DC machine used as DC Shunt Motor:
LF = 22 mH, RF + Radj = 220 − 250 Ω, V =450 V, LA =11.2mH, RA = 1.5 Ω, J = 0.55 kg/m2
Parameters of the induction machine used as motor: 6kW, 230/400V, 20/11A, 60 Hz, 1800 rpm, four poles, Rsm= 4.2Ω, Rrm= 1.99Ω, Lmm = 0.1600mH, B = 0.2985, Pm = 4, Lrm = 0.99 mH, L_{sm}=0.1700 mH, and J = 0. 80kg/m^2
Parameters of the LC filter: L=0.1e-3H, C=10μF.
Parameters of the Buck boost converter: C=350pF, L=12μH, Switching Frequency (F_S) =120 kHz.
Controller time constant T_M: 0.001 second.
Parameters of inverter: Nominal DC Voltage 450V, DC Power Rating 8kW, AC Power Rating 8kW. m_a= 0.8.

Appendix B

Table B1. The polynomial's Constants for approximating the output characteristics of the PV generator for the used three solar irradiance levels

Constants	Full solar Intensity	75% of full solar intensity	50% of full solar intensity
α1	- 0.0000000008636537367	- 0.00000001464237916	- 0.0000001313533287
α2	+0.0000001503117164	+ 0.000001911287808	+ 0.00001371656958
α3	-0.00001112257413	- 0.0001060717729	- 0.0006089887028
α4	+0.0004561386739	+ 0.003262516209	+ 0.01498483873
α5	- 0.01132890112	- 0.0607721823	- 0.2233028234
α6	0.1748581015	+ 0.7034999455	+ 2.067966206
α7	- 1.655448487	- 4.995227176	- 11.74693594
α8	+ 9.129147526	+ 20.66003541	38.86783987
α9	-26.33237834	- 44.69430476	- 67.26691591
α10	+ 29.73343113	37.85021854	+ 45.57300947
α11	+ 577.6724652	551.5263838	+ 531.2459074

Table B2. The polynomial's Constants for approximating the output characteristics of the magnetization curve of ferromagnetic material of DC Shunt Motor characteristics.

Constants of the polynomials that approximate the magnetization curve for ferromagnetic material of DC Shunt Motor	
α1	-0.000000000000000000000945
α2	0.00000000000000009999
α3	-0.00000999999999
α4	0.444444445555555
α5	-0.55555552
α6	-0.3094
α7	+1.1283
α8	+0.005

REFERENCES

[1] Mohammed I. Abuashour, et al., "Modeling, Simulations and Operational Performance of a Stand-Alone Hybrid Wind/PV Energy System Supplying Induction Motor for Pumping Applications," *Int. J. Engineering Systems Modelling and Simulation*, vol. 10, no. 1, pp. 12-25, 2018
[2] Doaa M. Atia1, et al., "Modeling and Control PV-Wind Hybrid System Based On Fuzzy Logic Control Technique," *Telecommunication Computing Electronics and Control*, vol. 10, no. 3, pp. 431-441, 2012.
[3] Mahmoud, H.A. and Nashed, M.N., "Solar Powered PV Stand-alone based DC Motor Drive using Fuzzy Logic Control," *International Journal of Engineering Research*, vol. 5, pp. 420-424, 2016.
[4] Sridhar R., et al., "Performance Analysis of a Standalone PV System with Reduced Switch Cascaded Multilevel Inverter," *International Journal of Power and Energy Conversion*, vol. 6, pp. 107-127, 2015.
[5] Widyan M.S., et al., "Transient Analysis and Output Characteristics of DC Motors Fed by Photovoltaic Systems," *Jordan Journal of Mechanical and Industrial Engineering*, vol. 4, pp. 193-204, 2010.
[6] T.O. Sweidan and M.S. Widyan, "Perturbation and Observation as MPPT Algorithm Applied on the Transient Analysis of PV-Powered DC Series Motor," *8th International Renewable Energy Congress (IREC)*, pp. 21-23, 2017.
[7] T.O. Sweidan, "Dynamical Analysis of DC Shunt Motor Powered by PV Generator Using Perturbation and Observation as MPPT Techniqu," *Energy and Power Engineering Journal (EPE)*, vol. 9, pp. 55-69, 2017.
[8] A. Z. Adnan, et al., "Analysis on the Impact of Renewable Energy to Power System Fault Level," *Indonesian Journal of Electrical Engineering and Computer Science*, vol. 11, no. 2, pp. 652-657, 2018.
[9] M. R. Patel, "Wind and Solar Power System," CRC Press LLC, 1999.
[10] H. S. Rauschenbach, "Solar Cell Array Design Handbook," Van Nostrand Reinhold, 1980.

[11] Mohammad S. Widyan, "Operational Performance of Synchronous Generator Hybrid-Excited by PMDC and PV Generators," *International Review of Electrical Engineering (I.R.E.E)*, vol. 9, no. 4, 2014.
[12] Ong, C.-M., "Dynamic Simulation of Electric Machinery," Prentice Hall PTR, Upper Saddle River, New Jersey 1998.
[13] Kundur P, "Power System Stability and Control," Mcgraw-Hill, New York 1994.
[14] Mohan N, "Power Electronics, Converters, Applications and Design," John Wiley & Sons, Inc., Chicago 2003.
[15] Jain S and Agarwal V, "Comparison of the Performance of Maximum Power Point Tracking Schemes Applied to Single-Stage Grid-Connected Photovoltaic Systems," *IET Electric Power Applications*, vol. 1, pp. 753-762, 2007.

BIOGRAPHIES OF AUTHORS

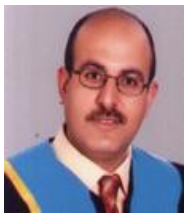

Mohammed I. Abuashour received his BSc in Electrical Engineering from the Jordan University of Science and Technology in 2009 and MSc in Electrical Power Engineering from the Yarmouk University, Jordan in 2016. He is working in the Electrical Engineering Department at The Hashemite University, Jordan since 2009 as an Engineer and Instructor. His fields of interest are power system stability, renewable energy systems integration, electrical machines dynamics, and electrical drives.

Tha'er O. Sweidan received his BSc in Electrical Engineering from the Hashemite University, Jordan in 2011 and MSc in Electrical Power Engineering from the Yarmouk University, Jordan in 2015. He worked in the Electrical Engineering Department at The Hashemite University, Jordan as Electrical Engineer and instructor from Feb 2012 to May 2018. Now Tha'er is working at Higher colleges of technology in Sharjah Women's College, in UAE as Lab Instructor since May 2018. His fields of interest are power system and electrical machine dynamics and optimization of renewable energy systems techniques.

Mohammad S. Widyan received his BSc in Electrical Power Engineering from the Yarmouk University, Jordan in 2000 and MSc in Control and Power Engineering from the Jordan University of Science and Technology in 2002. He received his PhD degree from the Berlin University of Technology, Germany in 2006. Currently, he is an Associate Professor of Electrical Engineering at The Hashemite University. His fields of interest are power system and electrical machine dynamics, bifurcation theory and control, permanent-magnet and conventional electrical machine design, finite element technique and renewable energy systems.

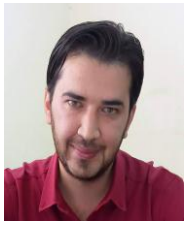

Mohammed M. Alhattab received his BSc in Electrical Engineering from the Hashemite University, Jordan in 2012 and MSc in Electrical Power Engineering from the Yarmouk University, Jordan in 2017. He has joined Electrical Engineering Department at The Hashemite University, Jordan since 2013 as a Lab Engineer (instructor of many labs such as: electrical circuits, electronics, machines, and renewable energy labs). His fields of interest are power system stability, power electronics, electrical machines and load forecasting.

Mohammed A. AlMai'tah received his BSc in Electrical Engineering from the Hashemite University, Jordan in 2007 and MSc in Electrical Power Engineering from the Yarmouk University, Jordan in 2016. He has joined Electrical Engineering Department at The Hashemite University, Jordan since 2007 as Lab instructor. His fields of interest are power system stability, power electronics, electrical -machines and load forecasting.